AD-A137 388 CRACK PATHS AND HYDROGEN-ASSISTED CRACK GROWTH RESPONSE IN AISI 4340 STEE.. (U) LEHIGH UNIV BETHLEHEM PA INST OF FRACTURE AND SOLID MECHANICS.. M GAO ET AL. SEP 83 1/1

UNCLASSIFIED IFSM-83-121 N00014-75-C-0543 F/G 11/6 NL

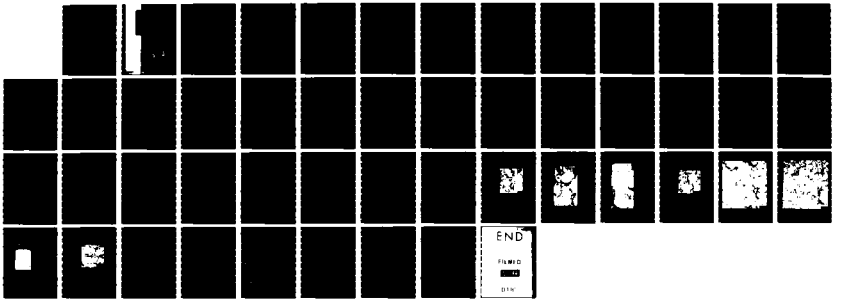

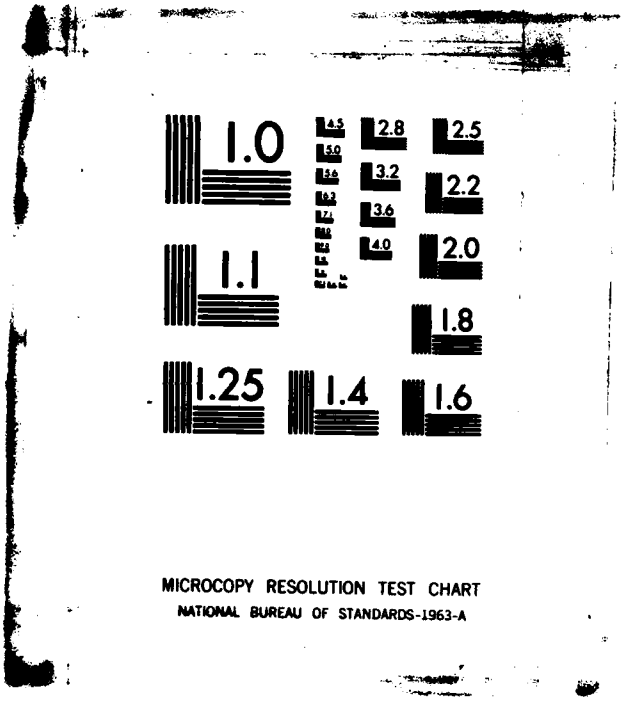
1.0
1.1
1.25
1.4
1.6
1.8
2.0
2.2
2.5
2.8
3.2
3.6
4.0
4.5
5.0
5.6
6.3
MICROCOPY RESOLUTION TEST CHART
NATIONAL BUREAU OF STANDARDS-1963-A

(12)

IFSM-83-121

LEHIGH UNIVERSITY

CRACK PATHS AND HYDROGEN-ASSISTED CRACK GROWTH REPONSE IN AISI 4340 STEEL

by

M. Gao, M. Lu, and R. P. Wei

September, 1983

Technical Report No. 15

Office of Naval Research

Contract N00014-75-C-0543, NR 036-097

CRACK PATHS AND HYDROGEN-ASSISTED CRACK GROWTH RESPONSE IN AISI 4340 STEEL

by

M. Gao[1], M. Lu[2] and R. P. Wei[3]
Lehigh University
Bethlehem, PA 18015

Technical Report No. 15

OFFICE OF NAVAL RESEARCH

[1] Visiting Scholar, Department of Metallurgy and Materials Engineering, on leave from the Department of Materials Science, Shanghai Jaio Tong University, Shanghai, People's Republic of China.

[2] Formerly Research Associate, Department of Mechanical Engineering and Mechanics.

[3] Professor of Mechanics, Department of Mechanical Engineering and Mechanics.

UNCLASSIFIED

SECURITY CLASSIFICATION OF THIS PAGE (When Data Entered)

REPORT DOCUMENTATION PAGE		READ INSTRUCTIONS BEFORE COMPLETING FORM
1. REPORT NUMBER IFSM-83-121	2. GOVT ACCESSION NO. AD-A137 388	3. RECIPIENT'S CATALOG NUMBER
4. TITLE (and Subtitle) CRACK PATHS AND HYDROGEN-ASSISTED CRACK GROWTH RESPONSE IN AISI 4340 STEEL		5. TYPE OF REPORT & PERIOD COVERED Technical Report No. 15 6. PERFORMING ORG. REPORT NUMBER
7. AUTHOR(s) M. Gao, M. Lu and R. P. Wei		8. CONTRACT OR GRANT NUMBER(s) Contract N00014-75-C-0543
9. PERFORMING ORGANIZATION NAME AND ADDRESS Lehigh University Bethlehem, PA 18015		10. PROGRAM ELEMENT, PROJECT, TASK AREA & WORK UNIT NUMBERS NR 036-997
11. CONTROLLING OFFICE NAME AND ADDRESS Office of Naval Research Department of the Navy Arlington, VA		12. REPORT DATE September, 1983 13. NUMBER OF PAGES 47
14. MONITORING AGENCY NAME & ADDRESS(if different from Controlling Office)		15. SECURITY CLASS. (of this report) Unclassified 15a. DECLASSIFICATION/DOWNGRADING SCHEDULE

16. DISTRIBUTION STATEMENT (of this Report)

This document has been approved for public release and sale; its distribution is unlimited.

17. DISTRIBUTION STATEMENT (of the abstract entered in Block 20, if different from Report)

18. SUPPLEMENTARY NOTES

19. KEY WORDS (Continue on reverse side if necessary and identify by block number)

Fracture mechanics, fractography, steels, hydrogen embrittlement microstructure.

20. ABSTRACT (Continue on reverse side if necessary and identify by block number)

A study of the correlation between crack paths and crack growth response was undertaken to better define the elemental processes involved in gaseous hydrogen embrittlement. AISI 4340 steel fractured under sustained load in hydrogen and in hydrogen sulfide over a range of temperatures and pressures, whose crack growth kinetics have been well characterized previously, was chosen for study. —>

DD FORM 1 JAN 73 1473 EDITION OF 1 NOV 65 IS OBSOLETE
S/N 0102-014-6601

UNCLASSIFIED

SECURITY CLASSIFICATION OF THIS PAGE (When Data Entered)

Fractographic results showed that crack growth followed predominantly along prior-austenite grain boundaries, with a small amount of quasi-cleavage, at low temperatures. At high temperatures, crack growth occurred primarily by microvoid coalescence. The fracture surface morphology, which is indicative of the micromechanisms for crack growth, was essentially the same for hydrogen and hydrogen sulfide. Changes in fracture morphology, i.e., crack paths, corresponded to changes in crack growth kinetics, both of which depended on pressure and temperature. There was no evidence for crack nucleation in advance of the main crack, and this suggests that the fracture process zone is located within one prior-austenite grain diameter from the crack tip.

The experimental results indicate that microstructure plays an important role in determining crack growth response. The prior-austenite grain boundaries are seen to be most susceptible to hydrogen embrittlement, followed by the $\{110\}_{\alpha'}$ and $\{112\}_{\alpha'}$ cleavage planes. The martensite matrix, on the other hand, is relatively immune. The observed changes in crack growth rate with temperature and pressure in the higher temperature region are explained in terms of the partitioning of hydrogen into the different microstructural elements and the consequent changes in the micromechanisms for fracture.

CRACK PATHS AND HYDROGEN-ASSISTED CRACK GROWTH RESPONSE IN AISI 4340 STEEL

M. Gao[1], M. Lu[2], and R. P. Wei[3]
Lehigh University
Bethlehem, PA 18015

ABSTRACT

A study of the correlation between crack paths and crack growth response was undertaken to better define the elemental processes involved in gaseous hydrogen embrittlement. AISI 4340 steel fractured under sustained load in hydrogen and in hydrogen sulfide over a range of temperatures and pressures, whose crack growth kinetics have been well characterized previously. was chosen for study.

Fractographic results showed that crack growth followed predominantly along prior-austenite grain boundaries, with a small amount of quasi-cleavage, at low temperatures. At high temperatures, crack growth occurred primarily by microvoid coalescence. The fracture surface morphology, which is indicative of the micromechanisms for crack growth, was essentially the same

---

[1]Visiting Scholar, on leave from the Department of Materials Science, Shanghai Jaio Tong University, Shanghai, People's Republic of China.

[2]Formerly Research Associate, Department of Mechanical Engineering and Mechanics.

[3]Professor of Mechanics, Deparment of Mechanical Engineering and Mechanics.

for hydrogen and hydrogen sulfide. Changes in fracture morphology, i.e., crack paths, corresponded to changes in crack growth kinetics, both of which depended on pressure and temperature. There was no evidence for crack nucleation in advance of the main crack, and this suggests that the fracture process zone is located within one prior-austenite grain diameter from the crack tip.

The experimental results indicate that microstructure plays an important role in determining crack growth response. The prior-austenite grain boundaries are seen to be most susceptible to hydrogen embrittlement, followed by the $\{110\}_{\alpha'}$ and $\{112\}_{\alpha'}$ cleavage planes. The martensite matrix, on the other hand, is relatively immune. The observed changes in crack growth rate with temperature and pressure in the higher temperature region are explained in terms of the partitioning of hydrogen into the different microstructural elements and the consequent changes in the micromechanisms for fracture.

1. INTRODUCTION

It is well known that high-strength steels exposed to hydrogen-bearing environment exhibit high susceptibility to hydrogen embrittlement under sustained load. Studies of crack growth in hydrogen and hydrogen sulfide have indicated that the kinetics of Stage II crack growth show substantially different response in two temperature regions [1-5] (see Section 3 and Figs. 1 and 2). At "low" temperatures, crack growth reflects control by transport of gases to the crack tip (or external transport) or reaction of the gas with newly created surfaces at the crack tip, or hydrogen diffusion(or internal transport) to the embrittlement region ahead of the crack tip. The crack growth rates conform to the temperature and pressure dependence of the rate controlling process [3-6]. The transfer of control from one process to another and the resultant change in crack growth rates, as one changes environmental conditions in the "low" temperature region, are reasonably well understood [6].

At "high" temperatures, the crack growth rates are substantially lower than those predicted by the low-temperature rate controlling process if it had remained in control. The reasons for the decrease in growth rate with increasing temperatures in this region, however, are less clear. The decrease may result from a decrease in the rate of supply of hydrogen engendered by changes occurring outside of the steel [1,2], or from a phase transformation at clean fracture surfaces [7], or from changes in fracture paths caused by the distribution of hydrogen into different regions of microstructure.

Clarification of this issue is essential to the further understanding of rate controlling processes for Stage II crack growth response and of hydrogen embrittlement mechanisms.

Hydrogen embrittlement apparently involves a region of material ahead of the crack tip. In other words, it occurs by a "volume embrittlement" mechanism as opposed to a "surface" mechanism [8-11]. This volume embrittlement, or reduction in local fracture stress, results from interactions of the microstructure with the deleterious species (e.g., hydrogen) that enter the material to reduce the interatomic bond strength, or to alter the local chemistry or microstructure. As a result of these interactions, cracks tend to follow specific paths through the microstructure. The particular paths and rates of growth are expected to depend on the local concentration of the deleterious species on and the rate of supply of these species to the various fracture sites. The paths, therefore, are expected to depend on temperature and pressure of the environment. Changes in fracture surface morphology or crack paths with environmental conditions have been recognized previously [7]. Their role in altering crack growth response, however, has not been systematically studied.

Since fractographic analysis has served as a powerful tool for defining the elemental prcoesses involved in fracture, this technique is often used in conjunction with stress corrosion cracking or hydrogen embrittlement tests. Some fundamental characteristics of fracture surfaces, produced by hydrogen assisted crack growth or embrittlement have been identified [7,

12-19]. In high-strength steels, hydrogen-assisted subcritical crack growth is often characterized by intergranular separation and by transgranular cleavage and quasi-cleavage [2,20,21]. In addition, transgranular failure by microvoid coalescence has also been observed [16,20,22,23]. These quite different and apparently contradictory findings may have resulted from the fact that many of the variables, which can affect the mode of hydrogen-assisted crack growth, were different in the various studies. Clearly, to advance the state of understanding, fractographic analysis must be carried out in conjunction with well controlled crack growth experiments, and must be correlated with the observed crack growth response.

Furthermore, in developing suitable models for gaseous hydrogen embrittlement, it is essential to establish the location of the fracture process zone (FPZ). Models based on the critical role of stress in gaseous hydrogen embrittlement suggested that the FPZ can be either at the crack tip (surface mechanism) [8,9] or at some distance away from the crack tip (volume embrittlement) [10,11]. On the other hand, it has been suggested that hydrogen assisted fracture may occur in a "near surface region" in between the crack tip and the maximum depth of hydrogen transport by diffusion. The size of this region is estimated to be of the order of 1 to 10 pct of the plane strain plastic zone size [24,25]. Thus, the location of FPZ requires further investigation.

In the present study, an experimental program was undertaken to better define the elemental processes involved in environmentally assisted fracture. Specifically, cracking of

AISI 4340 steel under sustained load in hydrogen and in hydrogen sulfide over a range of temperatures and pressures was selected for study, because the crack growth kinetics have been well characterized previously [3,4]. In addition, a special experiment was devised to determine whether there is crack nucleation well ahead of the main crack. The results are considered in relation to the crack growth kinetics, and to the mechanism and rate controlling processes for crack growth.

2. MATERIAL AND EXPERIMENTAL WORK

The primary effort was directed towards examinations of (1) the crack paths associated with subcritical crack growth kinetics in hydrogen and hydrogen sulfide through the microstructure, and (2) the location of the fracture process zone. Since examinations of crack paths were carried out on specimens that had been used in previous studies on crack growth [3,4], only those procedures that are new to this study are described.

A laboratory vacuum melted AISI 4340 steel, with extra low residual impurity content, was used [3,4]. The chemical composition, heat treatment and room temperature tensile properties of this steel are given in Table 1.

Fracture surfaces produced from the kinetic studies [3,4] were examined with a scanning electron microscope (SEM), operated in the secondary electron imaging mode at 20 kV. The working distance was 16 mm, and most of the specimens were tilted 25 deg about an axis parallel to the direction of crack growth. In all cases, the complete fracture half of each modified WOL specimen (with thickness of 6.4 mm and width of 52.3 mm) was placed into

the microscope for examination, thus eliminating artifacts that might be introduced by sample sectioning. All of the fractographs were obtained from areas near the mid-thickness region of the specimens. The location of each of the areas of interest, with respect to the crack starter notch, was measured with the aid of the micrometer stage of the microscope so that the corresponding stress intensity factor K can be established.

To determine the extent of crack nucleation ahead of the main crack, a special experiment was devised. In this experiment, sustained-load crack growth was commenced in hydrogen sulfide and was interrupted following about 10 mm of growth. At the point of interruption, $K = 38$ MPa-$m^{1/2}$. The environmental chamber was then evacuated, and the specimen was baked out in vacuum (at about 10^{-7} Pa) at 373 K for 24 h to remove dissolved hydrogen. The crack was then extended about 2.5 mm by fatigue in vacuum to reveal features of the crack front that were associated with prior crack growth in hydrogen sulfide. The procedure was repeated (2.5 mm of growth in H_2S and 2.5 mm in vacuum), with $K = 45$ MPa-$m^{1/2}$ at the point of interruption, and the specimen was then fractured in air.

Fracture surfaces from this special experiment were then examined by SEM. Special attention was directed to the region along the hydrogen-sulfide/vacuum crack border to determine the extent of crack nucleation in advance of the main crack. Nucleation would be revealed by the presence of isolated intergranular or quasi-cleavage facets in the fatigue fracture surfaces produced in vacuum.

3. RESULTS

Detailed examinations of the fracture surface morphology (FSM) of AISI 4340 steel specimens tested in hydrogen and in hydrogen sulfide have been made by scanning electron microscopy (SEM). The results of these examinations are considered in relation to the different temperature regions of crack growth response (Figs. 1 and 2), namely, the "low" temperature region (Region A), the "high" temperature region (Region C) and the "transition" region (Region B).

3.1. General Features

Five failure modes are associated with cracking of AISI 4340 steel in hydrogen over Region A. These failure modes, illustrated in Fig. 3, are essentially the same as those for the maraging steels [7]; namely:

(i) A predominant component of intergranular separation along prior-austenite grain boundaries.

(ii) Grain facet markings and boundary phase cracking.

(iii) Microcracks out of the macroscopic plane of fracture (that is, secondary cracks) along prior-austenite grain boundaries.

(iv) A small amount of transgranular quasi-cleavage within the prior-austenite grains.

(v) A small amount of ductile tearing.

Of these, grain boundary or intergranular (IG) separation and quasi-cleavage (QC) are of primary interest.

The detailed features of intergranular separation may be seen from Fig. 4. The precisely matched microfractographs were taken from mating fracture surfaces and represent the area indicated by IG in Fig. 3. Two types of features are seen: (i) mating particle-and-hole pairs, as indicated by arrow 1, and (ii) certain characteristic markings, as indicated by arrow 2. The one-to-one matching of particle-and-hole pairs on mating grain facets suggest that these pairs are formed by hydrogen assisted cracking along the boundaries of residual phases.

There is considerable disagreement, however, regarding the origin for the observed characteristic grain facet markings. Wayman and Smith [26] suggested that these markings are related to the impingement of martensite laths at the prior-austenite boundaries. On the other hand, Williams and Nelson [20] considered them to be deformation evidenced on the prior austenite grain boundary facets. Beachem and Pelloux [16,27] defined the grain facet markings as tearing ridges, which resulted from plastic tearing of ligaments of material between growing microscopic cracks. From Fig. 4, the grain facet markings appear to be more like tear ridges (versus impingement of martensite laths), particularly since corresponding markings on the mating fracture surface are both convex.

The quasi-cleavage facets showed distinct geometrical markings, Fig. 5. These markings are related to the microstructural features of quenched and tempered martensite in AISI 4340 steel. The crystallographic features of these QC facets have been shown to be associated with cleavage along {110} planes in

martensite on the basis of etch pit and detailed crystallographic analyses. These analyses are reported in detail elsewhere [28]. The amount of quasi-cleavage on the fracture surfaces was small. For AISI 4340 steel cracked in hydrogen at 133 kPa and 270 K, for example, QC constituted only about 14 ±7 pct (estimated 95 pct confidence interval) of the fracture surface.

Fracture surface morphology of specimens cracked in hydrogen sulfide (i.e., for Stage II crack growth in Region A at both 0.133 and 2.66 kPa) is essentially identical with that for hydrogen, Fig. 6. The density of grain facet markings, and the amount of QC facets and of ductile tearing component is somewhat less than those observed in hydrogen. The reduced amount of these failure modes reflects the more severe embrittling effect of hydrogen sulfide [5,6,18].

Metallographic sections of fractured specimens were also examined. The results confirm the extensive hydrogen assisted separation along prior austenite boundaries and transgranular cracking observed by SEM. They also show extensive secondary grain boundary cracking and transgranular cracking in the region adjacent to the main crack.

3.2 Correlations of FSM with Crack Growth Kinetics

Effect of stress intensity factor on cracking in Region A

Observations made over a range of K_I values from 22 to 66 MPa-$m^{1/2}$ showed no gross changes in fracture modes as crack growth changed from Stage I to Stage II*. The density of grain

*The definition of Stage I and Stage II crack growths are given in Ref. [29].

facet markings and ductile tearing, however, increased slightly with increasing K_I, starting from the fatigue precrack on through Stage I and Stage II, up to the highest K_I levels investigated. This change is indicative of an increase in microscopic plastic deformation with increase in mechanical crack driving force. The amount of QC evidently was not affected by K_I level in the range studied. These results are consistent with those of maraging steels [7], but are in disagreement with those reported by Beachem [16] and Kerns [18].

Detailed examination of the border region between the fatigue precrack and the affected crack showed that there is no resolvable "stretch zone" associated with the onset of crack growth [19]. This result supports the suggestion that, in contradistinction to the case of lower strength steels, "plastic stretching" is not essential for the initiation of hydrogen embrittlement in high strength steels [7].

Effect of test temperature and pressure on the fracture morphology for Stage II cracking

Typical microfractographs taken from specimens tested in hydrogen at 133 kPa are shown in Fig. 7. These microfractographs show the changes in fracture surface morphology for Stage II crack growth with test temperature. The three lower temperatures correspond to the "low" temperature region, or Region A, of crack growth (see Fig. 1), and the highest temperature corresponds to Region C.

In the low temperature region (Region A), the Stage II crack rate follows an exponential relationship of Arrhenius type and is controlled by the rate of hydrogen-metal surface reaction [4].

Over this temperature range, the fracture modes are identical. They are predominently intergranular with respect to the prior-austenite grains, with a small amount of transgranular quasi-cleavage (Fig. 7a-c). In the high temperature region(Region C), crack growth rate deviates from and becomes less than that indicated by the extrapolation of the low-temperature Arrhenius-type relationship. The decrease in rate is accompanied by increasing amounts of transgranular dimpled separation with increases in temperature. The temperature at which the observed change in FSM begins is consistent with the temperature at which the crack growth rate starts to deviate from the Arrhenius relationship (i.e., a transition from Region A to Region C response). The implication of this correlation is discussed in Section 4.

The fracture surface morphology in Region C is characterized by the following four components:

(i) Transgranular dimpled rupture, some of which covers an area encompassing several prior-austenite grains. The amount of dimpled rupture increases with increasing temperature.

(ii) Intergranular (IG) separation along prior-austenite grain boundaries, with extensive grain facet markings. The amount of IG separation, in contradistinction to the dimpled failure, decreases with increasing temperature.

(iii) A small amount of transgranular quasi-cleavage (QC) separation. The QC component is completely replaced by the dimpled rupture component with increasing temperature in the early stages of Region C.

(iv) Intergranular and transgranular microcracks (that is, secondary cracking) out of the macroscopic fracture plane.

Similar to that for Region A, the Region C fracture morphology is essentially independent of stress intensity factor for the various hydrogen pressures. The only noticeable change in FSM is a small increase in the amount of dimpled rupture with increasing K_I.

The effect of hydrogen pressure on the fracture surface morphology at a given temperature is small. The temperature for the transition from IG and QC to MVC modes of separation, however, is obviously influenced by hydrogen pressure. For example, the first indication of MVC is observed at about 326K (52°C) for a hydrogen pressure of 133 kPa, and is about 286K (13°C) for 13.3 kPa. This fracture mode transition is again consistent with the effect of hydrogen pressure on the temperature for transition from Region A to Region C crack growth.

The effect of temperature on the FSM associated with crack growth in hydrogen sulfide is essentially identical to that for hydrogen (compare Figs. 7 and 8). At a hydrogen sulfide pressure of Ø.133 kPa, in Region A, the crack growth rate is proportional to $p/\sqrt{T}$ and is controlled by the rate of transport of H_2S to the crack tip. In this region, the FSM is the same as that for hydrogen in Region A and is unaffected by temperature. With increasing temperature, into Region C, the crack growth rate begins to deviate from the $p/\sqrt{T}$ relationship. A concommitant transition in FSM occurs with the amount of dimpled fracture

increasing with temperature. The transition from Region A to Region C occurs at about 320 K.

The fracture surface morphology associated with crack growth in hydrogen sulfide at 2.66 kPa shows the same features in Regions A and C as those seen in the corresponding regions at the lower pressure. The transition in FSM occurs within the range of 373 to 413 K at this pressure. It is significant to note that two different processes have been identified as rate controlling at 2.66 kPa in Region A [5]. Below about 293 K (22°C), crack growth is controlled by hydrogen diffusion. Beginning at about 293 K (22°C), there appears to be a transfer of control from hydrogen diffusion to gas transport, with the crack growth rate falling below that indicated by an Arrhenius-type relationship (Fig. 2). This transfer of control, however, is not accompanied by a change in fracture surface morphology, and resolvable amounts of dimpled rupture do not appear until the test temperature exceeds 373 K.

These fractographic observations on specimens tested in hydrogen and in hydrogen sulfide suggest that the fracture mode is unaffected by the rate controlling process for crack growth as long as an adequate amount of hydrogen is supplied. The transition from the IG and QC modes to the MVC mode of separation with increasing temperature was accompanied by significant reduction in crack growth rate. The temperature for fracture mode transition and the associated reduction in crack growth rate is dependent on hydrogen and hydrogen sulfide pressure. These changes may result from a temperature induced cut-off in hydrogen

supply [1,20] or from the repartitioning of hydrogen amongst the different microstructural sites. These possibilities are considered in Section 4.

3.3 Crack Nucleation Site and Fracture Process Zone

To establish the location of the FPZ, a special experiment is used to determine the extent of crack nucleation ahead of the main crack (see Section 2). Macrofractographs of fracture surfaces produced in this special experiment clearly delineates the different steps in the experimental sequence, Fig. 9. The SEM results confirm that the fracture surface morphology produced by crack growth under sustained load in hydrogen sulfide is completely different from that produced by fatigue in vacuum. Thus, the crack front contour and crack nucleation associated with crack growth in hydrogen sulfide can be easily identified. A typical region between fatigue in vacuum and sustained-load crack growth in H_2S is shown in Fig. 10. There is no evidence for crack nucleation in advance of the main crack. To confirm this observation, careful examinations of the entire crack front region for both low K_I and high K_I levels have been made by SEM and a series of microfractographs were taken. A map of such a region can be constructed from these microfractographs. A sketch of a part of this map is shown in Fig. 11. It can be seen that the crack front is quite irregular on the microscopic scale. Finger-like protrusions extend from the main crack front for several grain diameters, or for about 20 to 80 μm. There is, however, no evidence for isolated crack nuclei ahead of the crack front. The FPZ, therefore, is considered to be within one prior-austenite grain diameter of the crack tip. The reported evidence

for nucleation ahead of the main crack [29,30] may be an artifact of sectioning, or may be applicable only to the lower strength steels where significant crack blunting can occur.

4. DISCUSSION

4.1 Crack Paths and Crack Growth Kinetics (The Role of Microstructure)

Fractographic analyses from this study showed that temperature is the key variable in determining the crack path for hydrogen embrittlement of AISI 4340 steel. The change in the mean Stage II crack growth rate in going from temperature Region A to Region C, for AISI 4340 steel exposed to gaseous hydrogen at pressures of 13.3, 57 and 133 kPa, is correlated with a transition in fracture mode. The temperatures at which these changes took place depended on the hydrogen pressure. The change in FSM is difficult to explain in terms of the model proposed by Williams and Nelson [1,2,20]. According to their model, the low temperature branch of the kinetics curve is controlled by activated adsorption of hydrogen. The high temperature branch, on the other hand, is controlled by the equilibrium between adsorbed and gaseous hydrogen. If the associated change in hydrogen supply is the sole cause for change in crack response, then one should observe the same fracture surface morphology at the same crack growth rate in the two temperature regions, because the hydrogen supplied to the steel is expected to be equal. The observed difference in FSM, however, suggests that different micromechanisms or different hydrogen embrittlement processes need to be considered for the two temperature regions.

To examine the correlation between micromechanisms (crack paths) and crack growth response, one might divide the embrittlement sequence roughly into three portions. These three portions are depicted schematically in Fig. 12. The first portion is concerned with the supply of hydrogen, and includes gas phase transport, surface reactions, and entry and diffusion of hydrogen to the embrittlement sites. The second portion involves the partitioning of hydrogen among the potential fracture sites in the microstructure. These sites (i.e., the potential crack paths) in AISI 4340 steel include: (i) the prior-austenite grain boundaries, (ii) {110} and {112} planes through martensites [13,14,28,32], and (iii) the martensite lattice itself. The third portion deals with the embrittlement reaction at each type of site, with the prior-austenite grain boundaries being most susceptible and the martensite lattice least susceptible to hydrogen embrittlement. Cracking at the respective microstructural elements would depend on the concentration and rate of supply of hydrogen there. The overall crack growth rate would be determined by the rates of cracking through the participating microstructural elements.

It is reasonable to suggest that the partitioning or distribution of hydrogen to the different microstructural elements is a function of temperature and pressure. Hence, the concentration and rate of supply of hydrogen to the different fracture sites becomes functions of temperature and pressure. At low temperatures, most of the hydrogen concentrates at the prior-austenite boundaries and at the QC sites. The fracture is therefore predominantly intergranular, and includes a small amount of QC

cleavage. Because the rate of supply of hydrogen from the external environment is relatively low, crack growth is controlled by one of the hydrogen supply processes [3-6]. At the higher temperatures, or in Region C, more hydrogen is expected to go into the martensite lattice. Increasing amounts of microvoid coalescence or dimpled failure now occur with increasing temperature and result in slower crack growth rates. Accordingly, the changes in crack growth rate and crack growth response with temperature are attributed now to the transfer of micromechanisms of fracture instead of the process of hydrogen supply. The reduction in rate with temperature may be enhanced by gas-adsorbate equilibrium, which further reduces the availability of hydrogen at the more susceptible sites and elsewhere in the microstructure. The foregoing considerations are equally applicable to hydrogen and hydrogen sulfide.

Based on these considerations, preliminary modeling has been carried out [33]. The results suggest that Stage II crack growth rate can be expressed approximately as a function of temperature and pressure by Eqn. (1).

$$(da/dt)_{II} = \sum_i (\alpha_i f_i \kappa_i) \dot{Q}_t \qquad (1)$$

The subscript i in Eqn. (1) represents the i^{th} fracture mode, such as IG, QC and MVC. The other terms are defined as follows:

α_i = crack growth rate coefficient for the i^{th} mode.

f_i = areal fraction for the i^{th} mode.

κ_i = hydrogen distribution coefficient for the i^{th} mode; $\Sigma \kappa_i = 1$.

$\dot{Q}_t$ = rate of supply of hydrogen to the FPZ.

The rate of supply of hydrogen to the FPZ, for simplified cases, takes on the following form [3,4,6]:

For surface reaction control

$$\dot{Q}_t = C_s p_o^{1/2} \exp(-E_s/RT) \tag{2}$$

For transport control

$$\dot{Q}_t = C_t p_o/\sqrt{T} \tag{3}$$

For diffusion control

$$\dot{Q}_t = C_d p_o^{1/2} \exp(-E_d/2RT) \tag{4}$$

The hydrogen distribution coefficients, κ_i, may be derived by using either Boltzmann or Fermi-Dirac statistics [33]. These coefficients depend on the binding enthalpy (H_B) for hydrogen to the lattice defects (such as dislocations and grain boundaries) and the rate of supply of hydrogen to the different microstructural elements.

Based on Eqns. (1) to (4), and on reasonable estimates of H_B of about 90 kJ/mol and of other parameters, the temperature and pressure dependence for Stage II crack growth in high-strength steels was obtained [33]. The "predicted" dependence is consistent with expectations and appears to be in good agreement with the experimental results for AISI 4340 steel in both hydrogen and hydrogen sulfide from the previous studies [3-5,33] (see Figs. 1 and 2). Clearly, partitioning of hydrogen among the different microstructural elements plays an important role in determining the kinetics of crack growth and the crack growth response. This partitioning must be considered in addition to the considerations

of hydrogen supply; the latter being exemplified by that of Williams and Nelson [1,20].

4.2 Fracture Process Zone and Hydrogen Embrittlement

This part of the discussion is important to the question of how far hydrogen must penetrate into the steel ahead of the crack tip to induce cracking. Several investigators [30,31,34,35] have suggested that hydrogen must diffuse to the region of maximum stress triaxiality beyond the plastic enclave where crack nucleation takes place. Johnson [39], on the other hand, suggested that the site of crack nucleation is at the position of "maximum plastic triaxiality", which is well inside the plastic enclave and thereby requiring a much shorter diffusion distance. Neither case, however, is consistent with the experimental observations.

If microcrack initiation had occurred in a region beyond the plastic enclave [30,31,34,35], then a number of crack nuclei should have existed at a distance away from the crack tip; for example, 0.13 mm at K_I = 35 MPa-$m^{1/2}$ for AISI 4340 steel. The results of this study, however, showed no evidence for such crack nucleation ahead of the main crack. On the other hand, if initiation had taken place at the position of maximum plastic triaxiality [38,39], estimated to be at 10^{-5} to 10^{-4} mm from the crack tip for high strength steels, the isolated crack nuclei may not have been resolvable by scanning electron microscopy. The absence of isolated crack nuclei, therefore, does not rule out the initiation of microcracks at regions of high triaxiality. It suggests only that the initiation site would be very close to the crack tip.

It is interesting to note, however, that the assumption of crack nucleation at the site of maximum stress triaxiality (whether it be at the edge of the plastic enclave or well inside of the plastic zone, but close to the crack tip) would lead to K_I-dependent crack growth. This K_I dependence may be demonstrated by the following analysis for the case of diffusion controlled crack growth. Taking the distance from the crack nucleus to the tip of the main crack to be δ_t and the time required for each increment of crack growth to be t_{cr}, the rate of Stage II crack growth is given simply by Eqn. (5).

$$(da/dt)_{II} = \delta_t/t_{cr} \tag{5}$$

The time t_{cr} may be roughly estimated from Eqn. (6) by letting δ_t be equal to the diffusion distance for hydrogen [36].

$$t_{cr} = \delta_t^2/4D \tag{6}$$

where D is the diffusion coefficient for hydrogen in the matrix. Substitution of t_{cr} from Eqn. (6) into Eqn. (5) leads to the following expression for $(da/dt)_{II}$.

$$(da/dt)_{II} = 4D/\delta_t \tag{7}$$

Based on the assumption that cracks nucleate at the site of maximum stress triaxiality, the value of δ_t would be given by either Eqn. (8) or Eqn. (9).

$$\delta_t = K_I^2/\pi\sigma_{ys}^2 \qquad \text{(plastic zone size [37])} \tag{8}$$

$$\delta_t = K_I^2/2E\sigma_{ys} \qquad \text{(distance to the region of maximum plastic triaxiality [38])} \tag{9}$$

where E and σ_{ys} are the elastic modulus and yield strength of the material respectively. In either case, the crack growth rate would be inversely proportional to K_I^2; as shown by Eqn. (10).

$$(da/dt)_{II} = A(D/K_I^2) \qquad (10)$$

where A in Eqn. (10) is a proportionality constant. A similar equation may be derived directly from Johnson's diffusion model [39]. The predicted dependence on K_I from Eqn. (10) is clearly inconsistent with experimental observations of K_I-independent crack growth, and suggest that the assumption of advanced nucleation at the site of stress triaxiality, coupled with diffusion controlled growth, is not tenable.

The fact that no isolated nuclei exist in advance of the main crack does not mean that hydrogen embrittlement is a surface process. Based on results obtained in this study, one can only suggest that this nucleation would occur at a distance that is quite small with respect to the prior-austenite grain size and that the crack growth increment somehow remains constant at each critical time t_{cr}.

5. SUMMARY

A comprehensive program was undertaken to study the correlations of fracture surface morphologies with crack growth response, and to determine the extent crack of nucleation ahead of the main crack for AISI 4340 steel fractured under sustained load in hydrogen and in hydrogen sulfide. The principal results from this study are as follows:

1. The fracture surface morphology was essentially identical for hydrogen and hydrogen sulfide. For crack growth at "low" temperatures, the crack followed predominantly along prior austenite grain boundaries, with a small amount of quasi-cleavage separation. At the "high" temperatures, cracking occurred predominantly by intergranular separation and microvoid coalescence.
2. Fracture morphologies were independent of stress intensity factor and crack growth rate, through the Stages I and II transitions, for all temperature and pressure conditions studied.
3. Temperature was the key variable in determining the crack path for hydrogen embrittlement of AISI 4340 steel. The transition in fracture mode (i.e., crack path) was directly correlated with the temperature induced transition in mean Stage II crack growth rate. The temperatures at which these transitions take place depend on the hydrogen and hydrogen sulfide pressure.
4. There was no change in fracture surface morphology as the rate controlling process transfers from one to another. This fractographic observation supports the fact that transfer of control is not necessarily accompanied by a change in the micromechanism for embrittlement.
5. There was no evidence for isolated crack nuclei ahead of the main crack. Composites of microfractographs taken along the crack front showed that the crack front was

quite irregular on the microscopic scale. Fingerlike protrusions extend from the main crack front for several grain diameters.

These results suggest that the prior austenite grain boundaries, $\{110\}_{\alpha'}$ and $\{112\}_{\alpha'}$ planes of martensites, and the martensite lattice itself are potential fracture sites. The rate of cracking by each fracture mode appears to depend on the local concentration and rate of supply of hydrogen to these fracture sites. The crack growth rate and response, therefore, are expected to depend on temperature, pressure and the partitioning of hydrogen among these different microstructural elements. Crack growth response at high temperatures may be controlled by the fracture mechanism, or by the gas-adsorbate equilibrium, or both, whereas it is controlled by the hydrogen supply processes at low temperatures. The absence of isolated crack nuclei suggests that nucleation of cracks at the site of maximum triaxial stress is not a necessary condition for hydrogen assisted cracking. This nucleation would occur at a distance that is quite small with respect to the prior-austenite grain size and that distance somehow remains constant.

ACKNOWLEDGEMENT

This research was supported in part by the Office of Naval Research under Contract N00014-75-C-0543, NR 036-097.

REFERENCES

1. D. P. Williams and H. G. Nelson: Met. Trans., 1 (1970), p. 63.

2. H. G. Nelson, D. P. Williams and A. S. Tetelman: Met. Trans., 2, (1971), p. 953.

3. G. W. Simmons, P.S. Pao and R. P. Wei: Met. Trans. A, 9A, (1978), p. 1147.

4. M. Lu, P. S. Pao, N. H. Chan, K. Klier and R. P. Wei: in Proceedings of Second Japan Institute of Metals International Symposium (JIMIS-2), Hydrogen in Metals, Suppl. to Trans. Japan Inst. Metals, 21 (1980), p. 449.

5. M. Lu, P. S. Pao, T. W. Weir, G. W. Simmons and R. P. Wei: Met. Trans. A, 12A, (1981), p. 805.

6. R. P. Wei: in Hydrogen Effects of Metals, eds., I. M. Bernstein and Anthony W. Thompson, TMS-AIME, Warrendale, PA (1981), p. 677.

7. R. P. Gangloff and R. P. Wei: in Fractography in Failure Analysis, eds. B. M. Strauss and W. H. Cullen, Jr., ASTM STP 654, American Society for Testing and Materials, (1978), p.87.

8. R. A. Oriani: in Stress Corrosion Cracking and Hydrogen Embrittlement of Iron Base Alloys, eds. J. Hochmann, J. Slater and R. W. Staehle, NACE-5, Houston, TX (1978), p. 351.

9. R. A. Oriani: Berichte Bunsen-Gesellschaft fur Physik Chemie, 76, (1972), p. 848.

10. W. W. Gerberich, Y. T. Chan, and C. St. John: Met. Trans. A, 6A,(1975), p.1485.

11. W. W. Gerberich: in Hydrogen in Metals, eds. I. M. Bernstein and A. W. Thompson, American Society for Metals. Metals Park, OH, (1974), p. 115.

12. Shigehane Hinotani, Fukunaga Terasaki, and Fukukazu Natasato: in Proceedings of Second Japan Institute of Metals International Symposium (JIMIS-2), Hydrogen in Metals, Suppl. to Trans. Japan Inst. Metals, 21 (1980), p. 421.

13. Yoneo Kikuta, Takao Araki and Toshir Kutodo: in Fractography in Failure Analysis, eds. B. M. Strauss and W. H. Cullen, Jr., ASTM STP 645, American Society for Testing and Materials, (1978), p. 107.

14. Takao Araki and Yoneo Kikuta: in Proceedings of Second Japan Institute of Metals International Symposium (JIMIS-2), Hydrogen in Metals, Suppl. to Trans. Japan Inst. Metals, 21 (1980), p. 425.

15. J. P. Fidelle, J. Legrand and C. Couderc: "A Fractographic Study of Hydrogen Gas Embrittlement in Steels", TMS-AIME Paper No. F 71-81, (1971).

16. C. D. Beachem: Met. Trans., 3, (1972), p. 437.

17. R. A. Oriani and P. H. Josephic: Acta Met., 22. (1974), p. 1065.

18. G. E. Kerns: Ph. D. Dissertation, Ohio State University, Columbus, Ohio,(1973).

19. P. McIntyre: in Stress Corrosion Cracking and Hydrogen Embrittlement of Iron Base Alloys, eds., J. Hochmann, J. Slater and R. W. Staehle, NACE-5, Houston,TX, (1978), p. 788.

20. H. G. Nelson and D. P. Williams: in Stress Corrosion Cracking and Hydrogen Embrittlement of Iron Base Alloys, eds., J. Hochmann, J. Slater and R. W. Staehle, NACE-5, Houston, TX, (1978), p. 390.

21. A. J. Stavros and H. W. Paxton: Met. Trans., 1, (1970), p. 3049.

22. S. K. Banerji, H. C. Feng and C. J. McMahon, Jr.: Met. Trans. 9A, (1978), p. 237.

23. J. F. Lessar and W. W. Gerberich: Met. Trans. A, 7A, (1976), p. 953.

24. R. P. Gangloff: Ph.D. Dissertation, Lehigh University, Bethlehem, PA, (1974).

25. R. P. Gangloff and R. P. Wei: Met. Trans. A, 8A, (1977), p. 1043.

26. M. L. Wayman and G. C. Smith: Met. Trans. 1 (1970), p. 1189.

27. C. D. Beachem and R. M. N. Pelloux: in Fracture Toughness Testing and Its Application, ASTM STP 381, American Society for Testing and Materials, (1965), p. 210.

28. Ming Gao: M. S. Thesis in Metallurgy and Materials Engineering, Lehigh University, Bethlehem, PA (1982).

29. R. P. Wei, S. R. Novak and D. P. Williams: Matls. Res. & Stand., 12, (1972), p. 75.

30. H. H. Johnson, J. G. Morlet and A. R. Troiano: Trans. TMS-AIME, 212, (1958), p. 528.

31. J. Kameda and C. J. McMahon, Jr.: in Research in Progress, University of Pennsylvania, Philadelphia, PA, (Dec. 1979).

32. J. E. Costa and A. N. Thompson: Met. Trans. A, 12A, (1981), p. 761.

33. Ming Gao: Ph. D. Dissertation in Metallurgy and Materials Engineering, Lehigh University, Bethlehem, PA (1982).

34. T. D. Lee, T. Goldenberg and J. P. Hirth: Met. Trans. A, 10A, (1979), p. 439.

35. R. A. Oriani and P. H. Josephic: in Environment Sensitive Fracture of Engineering Materials, ed., Z. A. Foroulis, TMS-AIME, Warrendale, PA, (1979), p. 232

36. J. Crank: The Mathematics of Diffusion, Oxford University Press, (1976), p. 37.

37. A. A. Wells: Br. Weld. J., 10, (1963), p. 563.

38. J.R. Rice and M.A.Johnson: Inelastic Behavior of Solid, McGraw-Hill (1970), pp. 641-647.

39. H. H. Johnson: in Hydrogen in Metals, eds. I. M. Bernstein and A. W. Thompson, American Society for Metals, Metals Park, OH, (1974), p. 35.

TABLE 1

CHEMICAL COMPOSITION, HEAT TREATMENT, AND ROOM TEMPERATURE TENSILE PROPERTIES OF THE AISI 4340 STEEL INVESTIGATED

Chemical Composition (Weight Percent)

C	Mn	P	S	Si	Ni	Cr	Mo	Co	Ti
0.42	0.70	0.0009	0.0012	0.28	1.83	0.79	0.24	0.011	<0.005

Heat Treatment

Normalize, 1 h, 900°C, A.C. + austenitize, 1 h, 843°C, O.Q. + temper, 1 h, 204°C, A.C.

A.C. = air cool; O. Q. = oil quench

Tensile Properties

0.2% Offset Yield Strength MPa	Tensile Strength MPa	Young's Modulus GPa	Elongation Pct
1344	2082	201	9 (in 3.56 cm)

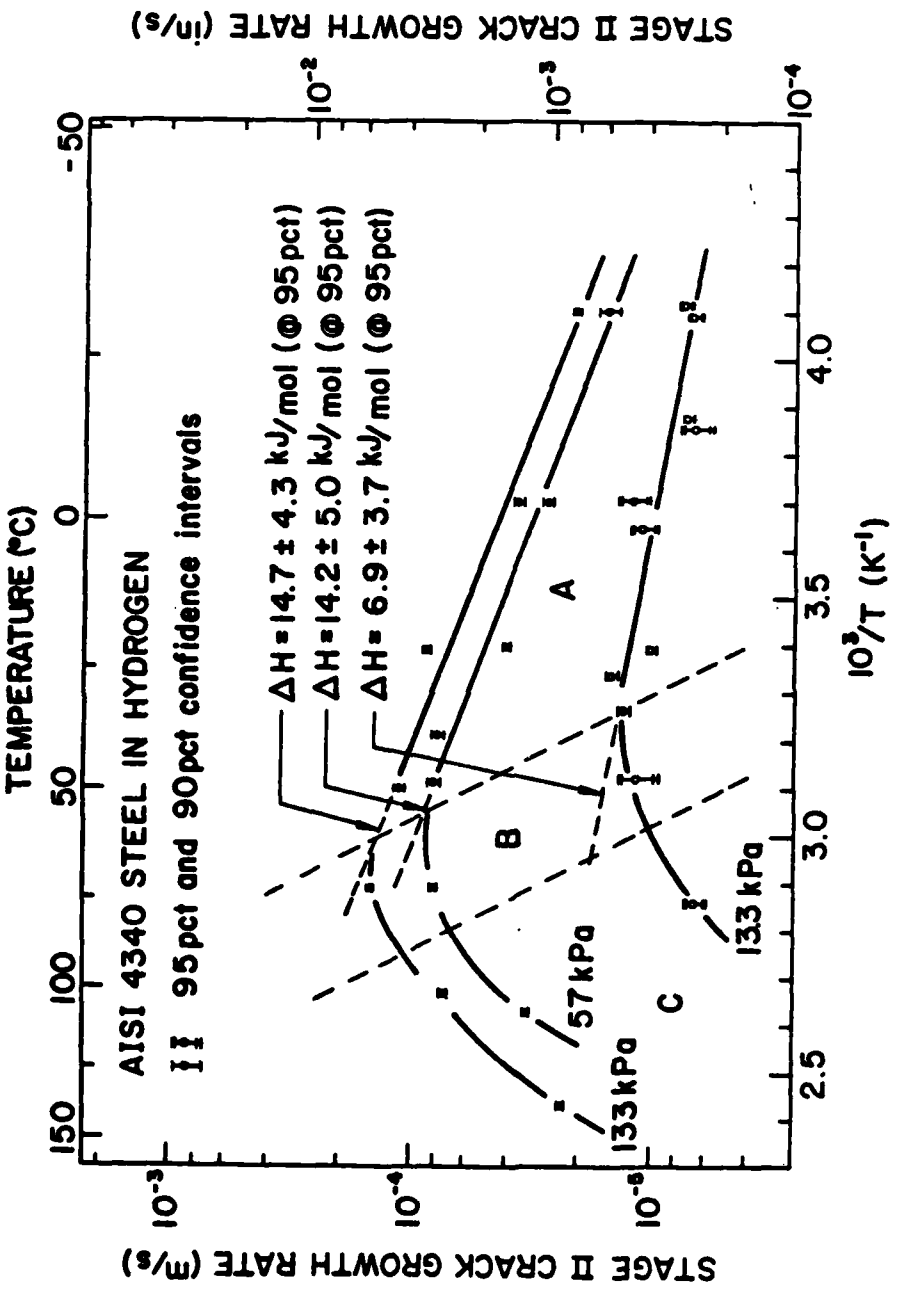

Figure 1: Effect of temperature on the rate of Stage II crack growth in AISI 4340 steel (tempered at 477 K) in dehumidified hydrogen at 13.3, 57 and 133 kPa. [3,4]

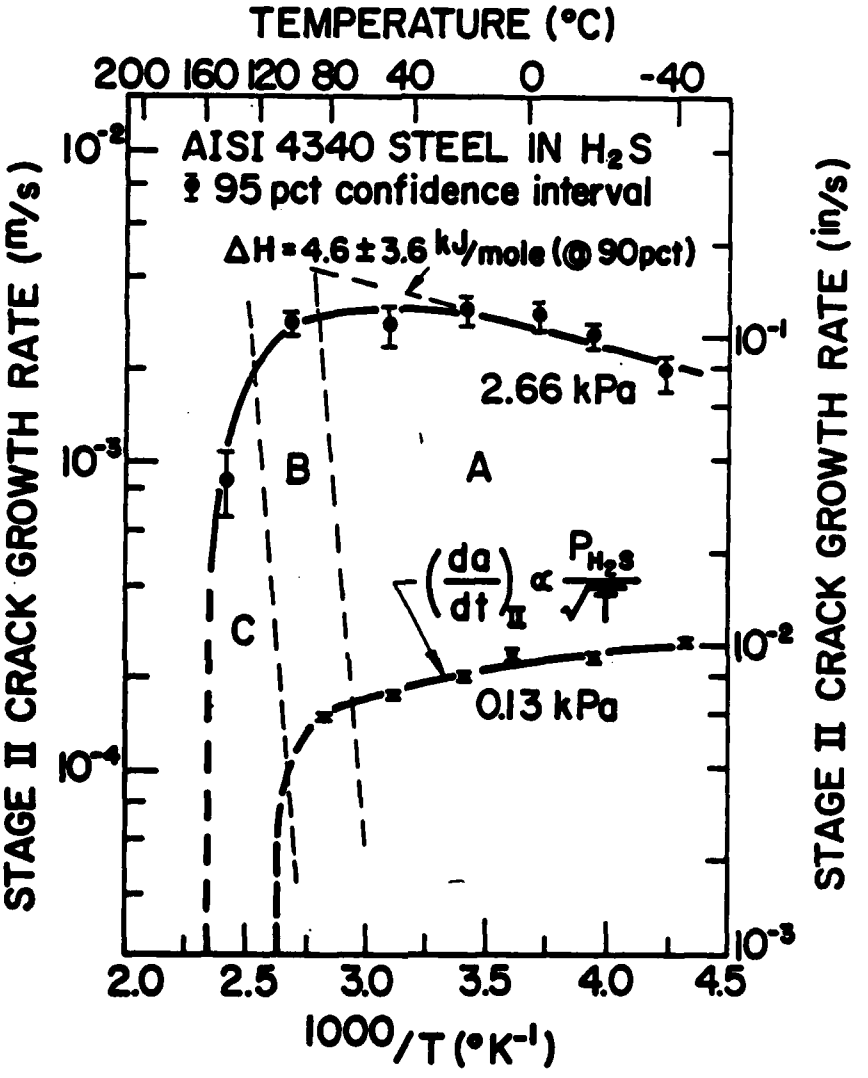

Figure 2: Effect of temperature on the rate of Stage II crack growth in AISI 4340 steel (tempered at 477 K) in hydrogen sulfide at 0.13 and 2.66 kPa. [5]

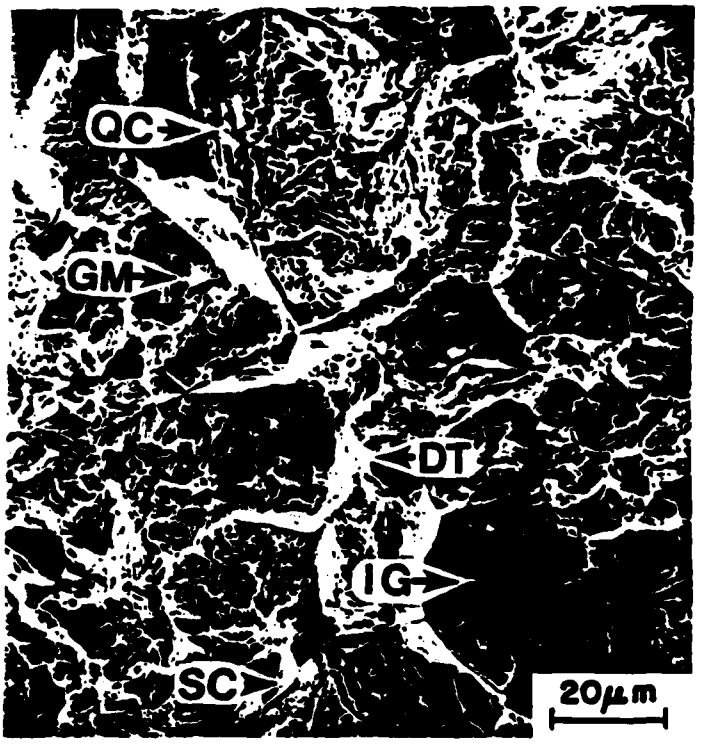

Figure 3: Scanning electron microfractograph of Stage II cracking in AISI 4340 steel exposed to hydrogen in Region A (p = 133 kPa, T = 296K). The arrows indicate intergranular separation (IG), quasi-cleavage (QC), secondary cracking (SC), grain boundary marking (GM), and ductile tearing (DT).

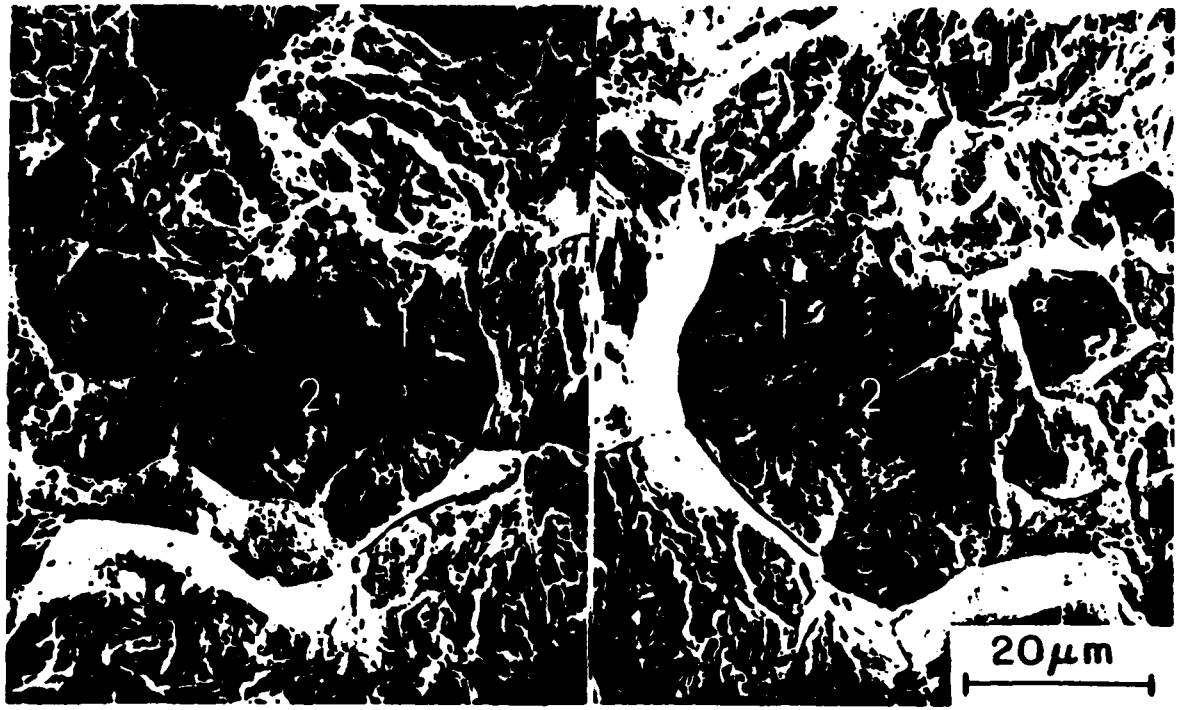

Figure 4: SEM microfractographs from mating fracture surfaces at area indicated by IG in Figure 3, showing intergranular separation, grain facet marking, boundary phase cracking and secondary cracking along prior austenite grain boundaries. (1-1 indicate a hole-particle pair and 2-2 a tear ridge pair.)

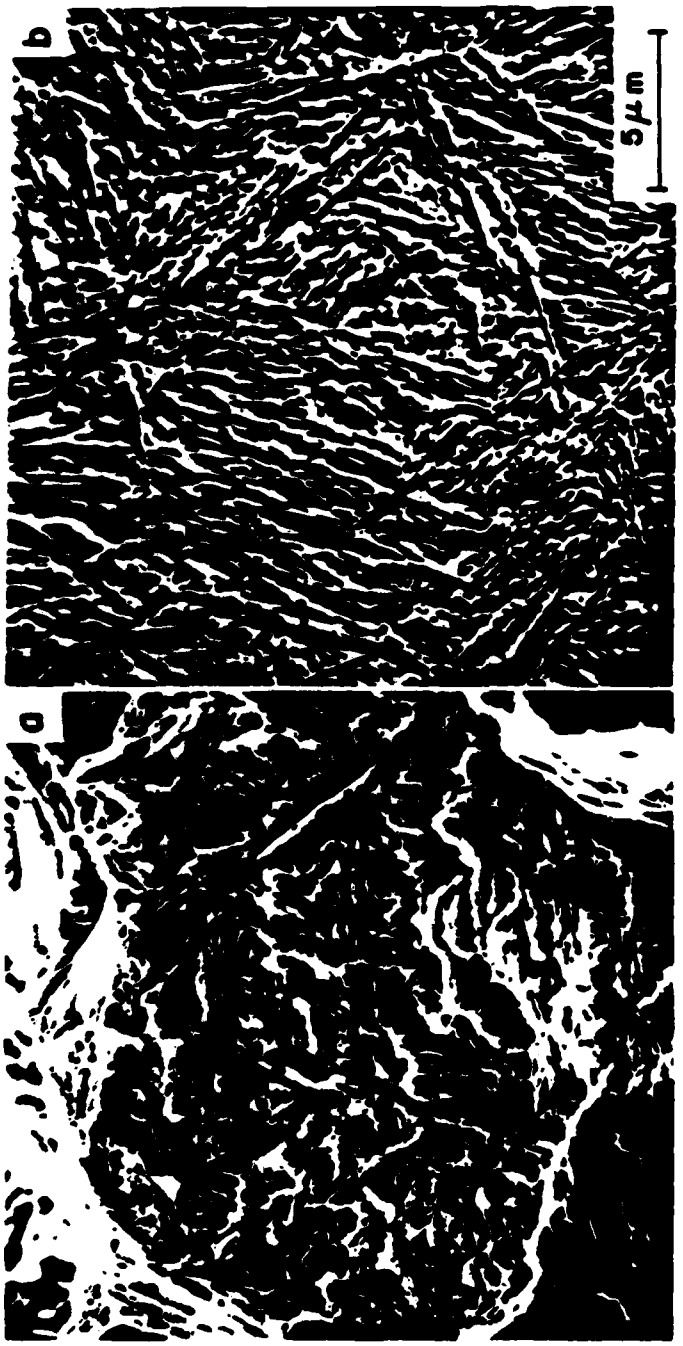

Figure 5: Comparison of the geometrical markings of quasi-cleavage facet produced by cracking in hydrogen and the microstructure of martensite in AISI 4340 steel.

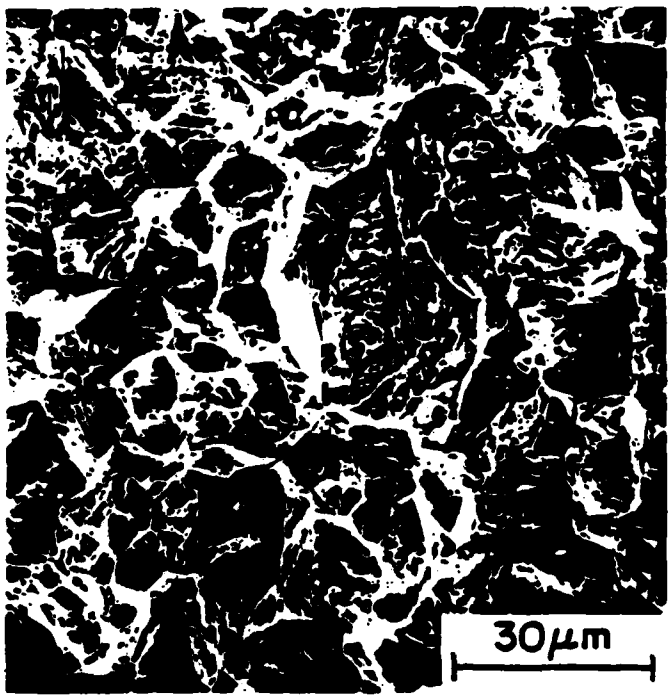

Figure 6: Scanning electron microfractograph of Stage II cracking in AISI 4340 steel exposed to hydrogen sulfide in Region A (p = 2.67 kPa; T = 296K; K = 44 MPa$\sqrt{m}$).

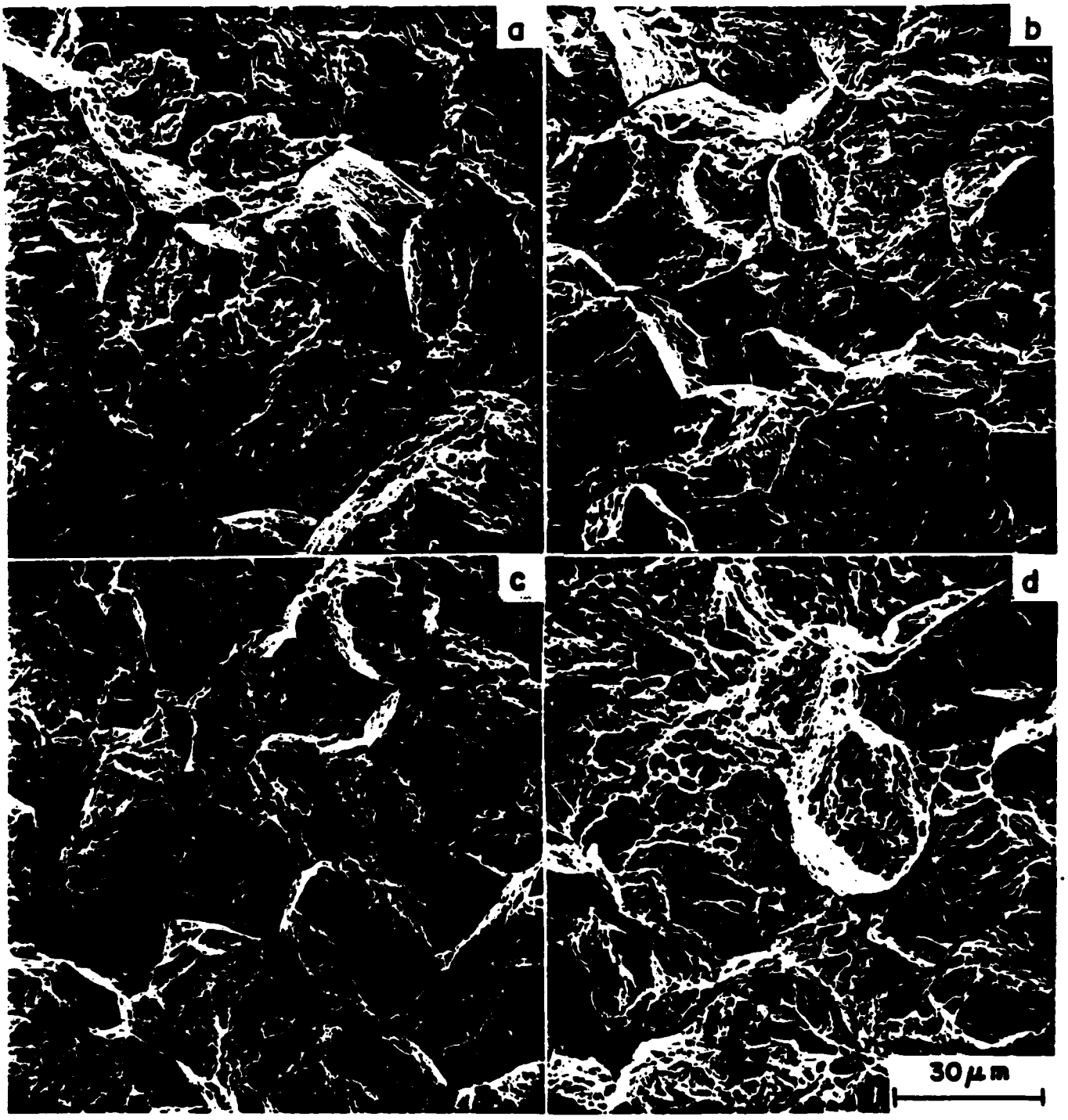

Figure 7: The influence of temperature on Stage II fracture surface morphology for hydrogen at 133 kPa: (a) 243K, (b) 295K, (c) 351K and (d) 412K.

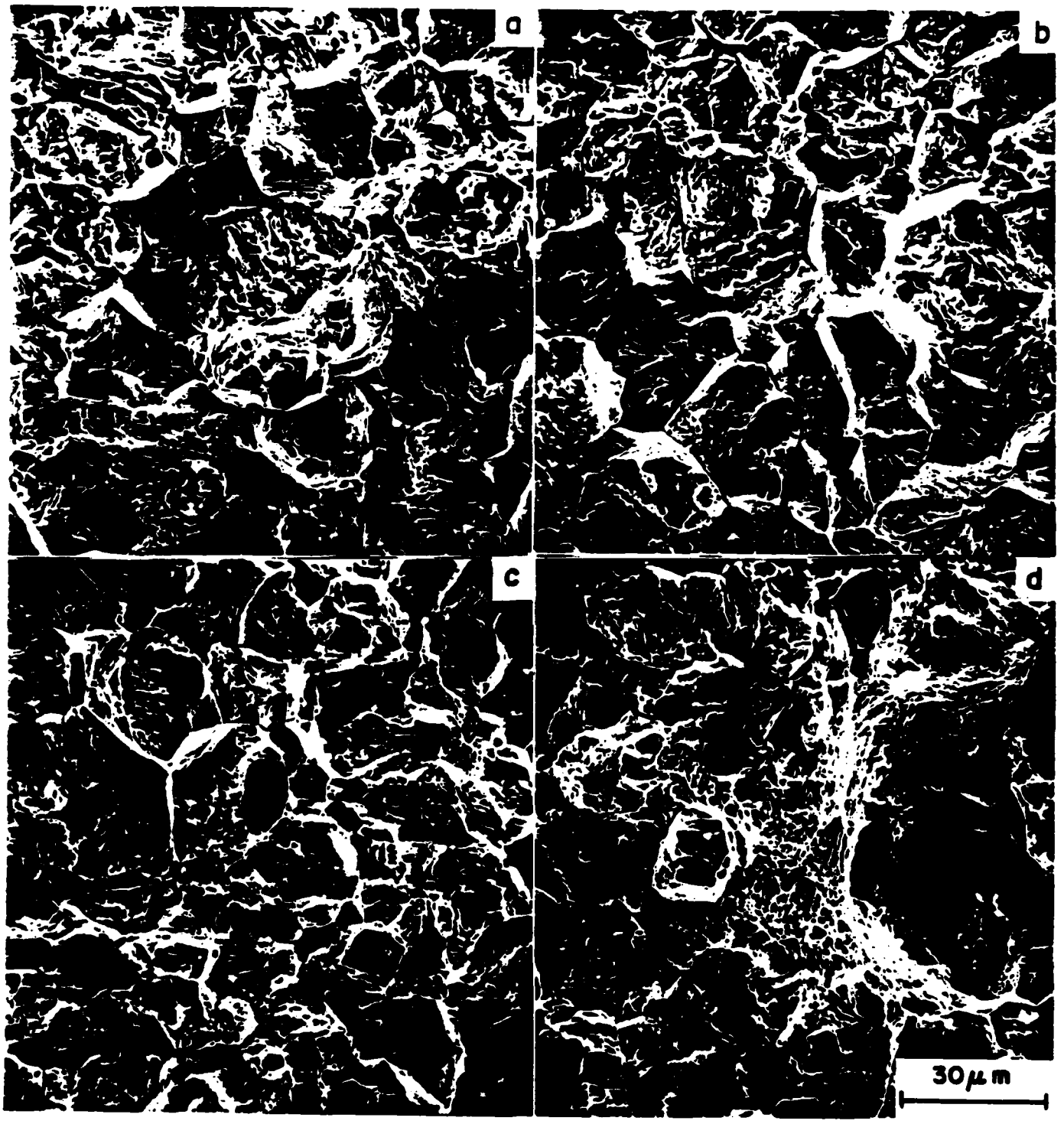

Figure 8: The influence of temperature on Stage II fracture surface morphology for hydrogen sulfide at 0.133 kPa: (a) 253K, (b) 276K, (c) 298K and (d) 353K.

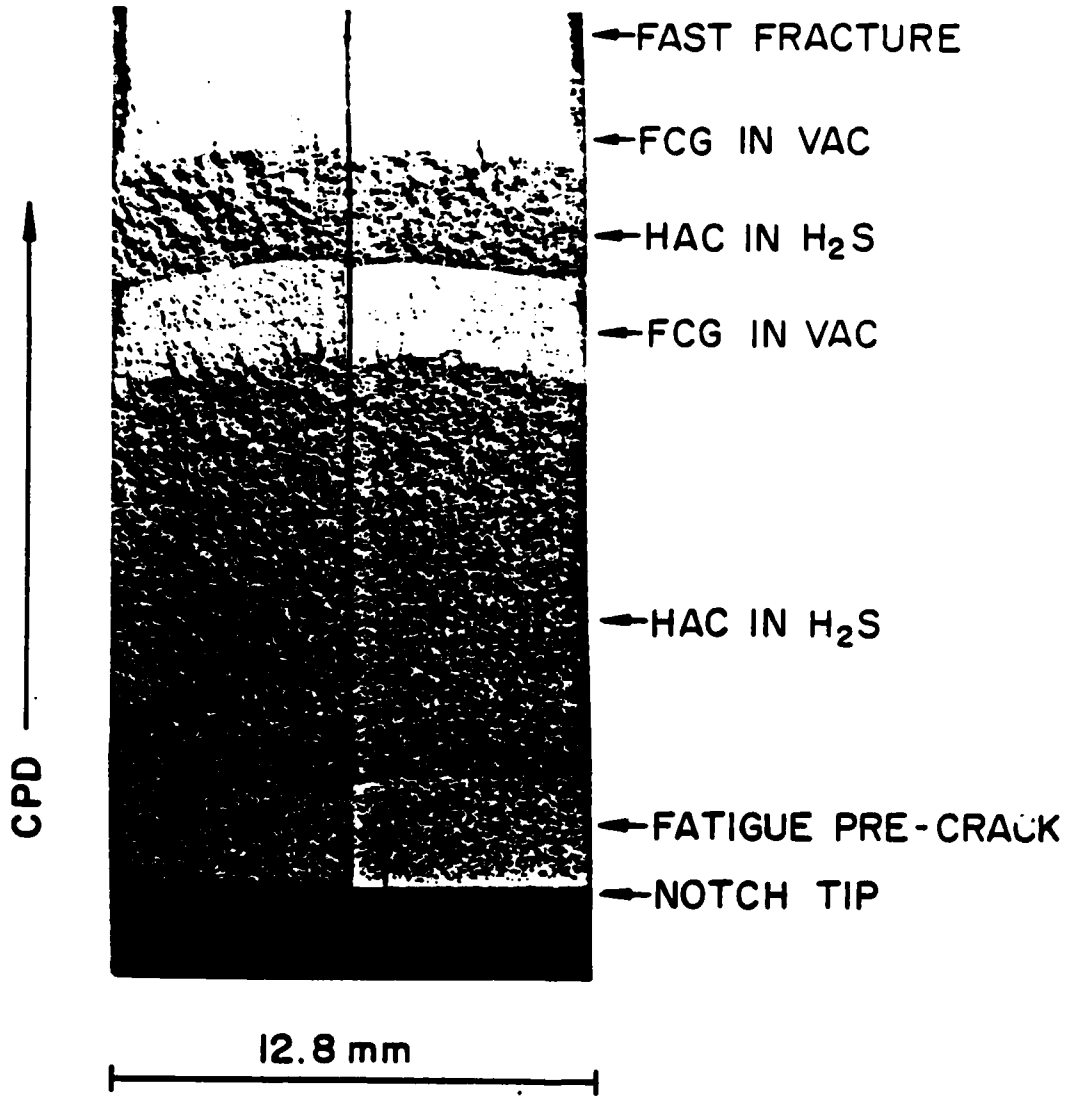

Figure 9: Macrofractograph of AISI 4340 steel tested in vacuum and in hydrogen sulfide at 0.067 kPa.

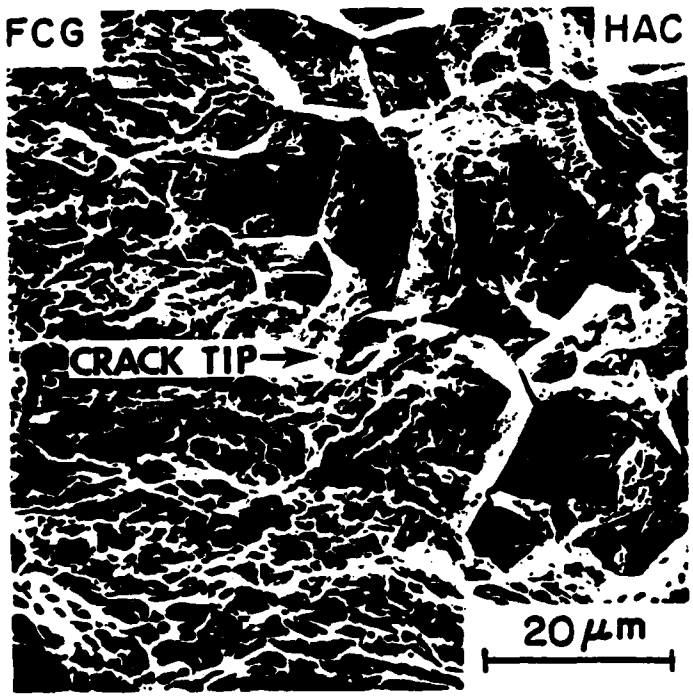

Figure 10: Scanning electron fractograph of a typical region between fracture in hydrogen sulfide under sustained load (HAC) and fracture by fatigue in vacuum at 1.3×10^{-4} Pa (FCG).

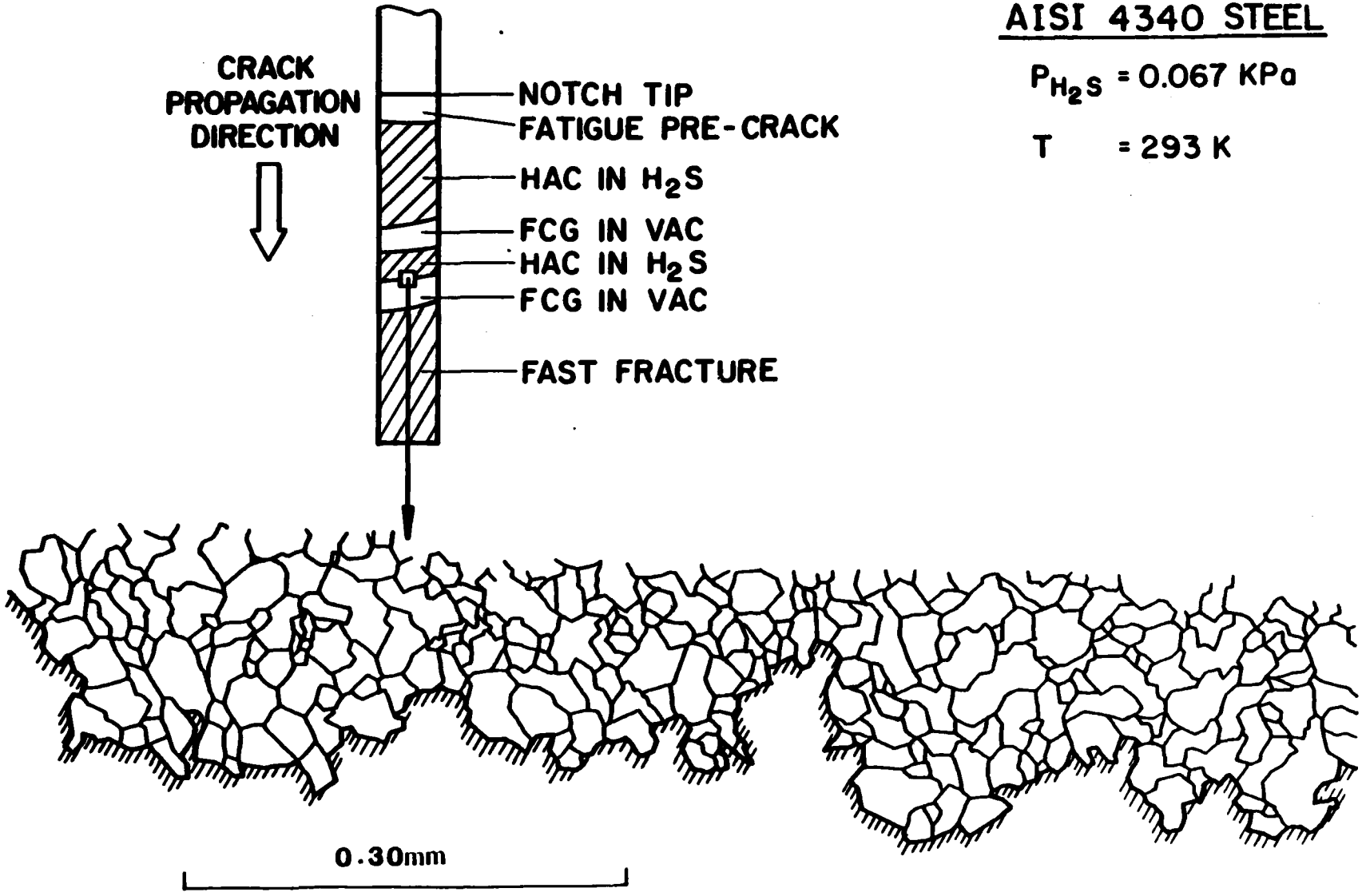

Figure 11: Sketch of crack front contour and fracture surface obtained from SEM microfractographs.

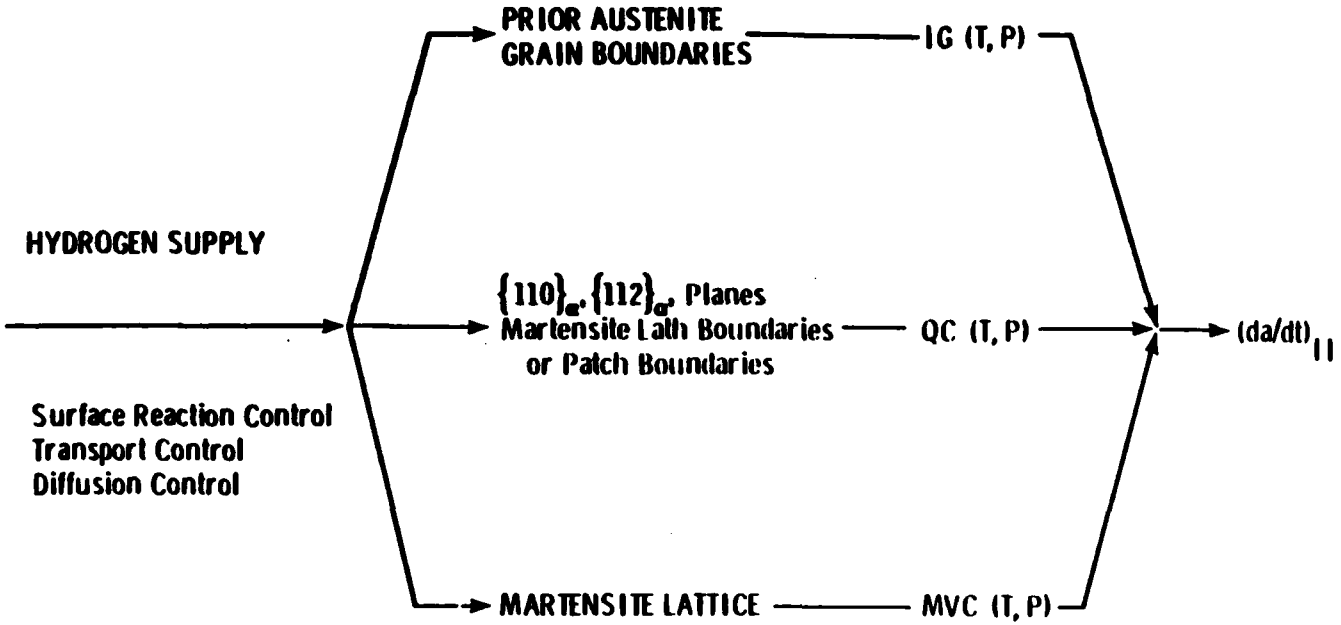

Figure 12 : Schematic illustration of hydrogen induced cracking steps.

BASIC DISTRIBUTION LIST

Technical and Summary Reports April 1978

Organization	Copies
Defense Documentation Center Cameron Station Alexandria, VA 22314	12
Office of Naval Research Department of the Navy 800 N. Quincy Street Arlington, VA 22217	
ATTN: Code 471	1
Code 102	1
Code 470	1
Commanding Officer Office of Naval Research Branch Office Building 114, Section D 666 Summer Street Boston, MA 02210	1
Commanding Officer Office of Naval Research Branch Office 536 South Clark Street Chicago, IL 60605	1
Office of Naval Research San Francisco Area Office One Hallidie Plaza Suite 601 San Francisco, CA 94102	1
Naval Research Laboratory Washington, DC 20375	
ATTN: Codes 6000	1
6100	1
6300	1
6400	1
2627	1
Naval Air Development Center Code 302 Warminster, PA 18964 ATTN: Mr. F. S. Williams	1

Organization	Copies
Naval Air Propulsion Test Center Trenton, NJ 08628 ATTN: Library	1
Naval Construction Batallion Civil Engineering Laboratory Port Hueneme, CA 93043 ATTN: Materials Division	1
Naval Electronics Laboratory San Diego, CA 92152 ATTN: Electron Materials Sciences Division	1
Naval Missile Center Materials Consultant Code 3312-1 Point Mugu, CA 92041	1
Commanding Officer Naval Surface Weapons Center White Oak Laboratory Silver Spring, MD 20910 ATTN: Library	1
David W. Taylor Naval Ship Research and Development Center Materials Department Annapolis, MD 21402	1
Naval Undersea Center San Diego, CA 92132 ATTN: Library	1
Naval Underwater System Center Newport, RI 02840 ATTN: Library	1
Naval Weapons Center China Lake, CA 93555 ATTN: Library	1
Naval Postgraduate School Monterey, CA 93940 ATTN: Mechanical Engineering Department	1

BASIC DISTRIBUTION LIST (cont'd)

Organization	Copies
Naval Air Systems Command Washington, DC 20360 ATTN: Codes 52031 52032	1
Naval Sea System Command Washington, DC 20362 ATTN: Code 035	1
Naval Facilities Engineering Command Alexandria, VA 22331 ATTN: Code 03	1
Scientific Advisor Commandant of the Marine Corps Washington, DC 20380 ATTN: Code AX	1
Naval Ship Engineering Center Department of the Navy Washington, DC 20360 ATTN: Code 6101	1
Army Research Office P.O. Box 12211 Triangle Park, NC 27709 ATTN: Metallurgy & Ceramics Program	1
Army Materials and Mechanics Research Center Watertown, MA 02172 ATTN: Research Programs Office	1
Air Force Office of Scientific Research Bldg. 410 Bolling Air Force Base Washington, DC 20332 ATTN: Chemical Science Directorate Electronics & Solid State Sciences Directorate	1 1
Air Force Materials Laboratory Wright-Patterson AFB Dayton, OH 45433	1
Library Building 50, Rm 134 Lawrence Radiation Laboratory Berkeley, CA	1

Organization	Copies
NASA Headquarters Washington, DC 20546 ATTN: Code RRM	1
NASA Lewis Research Center 21000 Brookpark Road Cleveland, OH 44135 ATTN: Library	1
National Bureau of Standards Washington, DC 20234 ATTN: Metallurgy Division Inorganic Materials Div.	1 1
Director Applied Physics Laboratory University of Washington 1013 Northeast Forthieth Street Seattle, WA 98105	1
Defense Metals and Ceramics Information Center Battelle Memorial Institute 505 King Avenue Columbus, OH 43201	1
Metals and Ceramics Division Oak Ridge National Laboratory P.O. Box X Oak Ridge, TN 37380	1
Los Alamos Scientific Laboratory P.O. Box 1663 Los Alamos, NM 87544 ATTN: Report Librarian	1
Argonne National Laboratory Metallurgy Division P.O. Box 229 Lemont, IL 60439	1
Brookhaven National Laboratory Technical Information Division Upton, Long Island New York 11973 ATTN: Research Library	1
Office of Naval Research Branch Office 1030 East Green Street Pasadena, CA 91106	1

DISTRIBUTION LIST
Corrosion Mechanisms

Professor J. P. Hirth
Ohio State University
Department of Metallurgical Engineering
1314 Kinnear Road
Columbus, OH 43212

Dr. J. Kruger
National Bureau of Standards
Washington, DC 20234

Dr. H. K. Birnbaum
University of Illinois
Department of Metallurgy and Mining Engineering
Urbana, IL 61801

Dr. D. J. Duquette
Rensselaer Polytechnic Institute
Department of Metallurgical Engineering
Troy, NY 12181

Dr. R. P. Wei
Lehigh University
Institute for Fracture and Solid Mechanics
Bethlehem, PA 18015

Prof. H. W. Pickering
Pennsylvania State University
Department of Material Science
University Park, PA 16802

Prof. I. M. Bernstein
Carnegi-Mellon University
Schenley Park
Pittsburg, PA 15213

Dr. T. R. Beck
Electrochemical Technology Corporation
10035 31st Avenue, N.E.
Seattle, WA 98125

Prof. R. T. Foley
The American University
Washington, DC 20016

Dr. D. L. Davidson
Southwest Research Institute
8500 Culebra Road
P.O. Box Drawer 28510
San Antonio, TX 78284

Dr. Barry C. Syrett
Stanford Research Institute
333 Ravenswood Avenue
Menlo Park, CA 94025

Prof. S. Weissmann
Rutgers, The State University
of New Jersey
College of Engineering
New Brunswick, NY 08903

Prof. H. Herman
State University of New York
Material Science Department
Stony Brook, NY 11794

Prof. R. M. Latanision
Massachusetts Institute of
Technology
77 Massachusetts Avenue, Room E19-702
Cambridge, MA 02139

Prof. E. A Starke. Jr.
Dept. of Materials Science
University of Virginia
Charlottesville, VA 22901

Prof. Morris E. Fine
Northwestern University
The Technological Institute
Evanston, IL 60201

Dr. C. S. Kortovich
TRW, Inc.
2355 Euclid Avenue
Cleveland, OH 44117

Dr. O. Buck
Rockwell International Science Center
1049 Camino Dos Rios
P.O. Box 1085
Thousand Oaks, CA 91360

Dr. R. J. Arsenault
University of Maryland
College Park,MD 20742

Dr. F. Mansfeld
Rockwell International (Science Ctr)
1049 Camino Dos Rios
P.O. Box 1085
Thousand Oaks, CA 91360

Continue of Distribution List

Dr. Paul Gordon
Illinois Institute of Technology
Department of Metallurgical and Materials
Engineering
Chicago, IL 60616

Dr. H. Leidheiser, Jr.
Lehigh University
Bethlehem, PA 18015

Dr. J. V. McArdle
University of Maryland
College Park, MD 20742

Dr. E. McCafferty
Naval Research Laboratory
Washington, DC 20375

Prof. J. G. Byrne
The University of Utah
Dept. of Materials Science & Engineering
Salt Lake City, Utah 84112

Prof. A. J. Ardell
University of California
School of Engineering and Applied Science
405 Hilgard Ave.
Los Angeles, CA 90024

Prof. J. A. S. Green
Martin Marietta Corporation
1450 South Rolling Road
Baltimore, MD 21227

Prof. G.H. Meier & F.S. Pettit
University of Pittsburgh
Dept. of Matallurgical and Materials
Engineering
Pittsburgh, PA 15261

Prof. Alexander M. Cruickshank
Gordon Research Conference
Pastore Chemical Laboratory
University of Rhode Island
Kingston, RI 02881

Dr. Theordore R. Beck
Electrochemical Technology Corp
3935 Leary Way NW
Seattle, Washington 98107

END

FILMED

02 — 84

DTIC